Infrared Telescope Facility's Spectrograph Observations of Human-Made Space Objects

Kira Abercromby
California Polytechnic State University, San Luis Obispo
Brent Buckalew
JACOBS
Paul Abell
NASA JSC
Heather Cowardin
JACOBS JETS, University of Texas El Paso

ABSTRACT

Presented here are the results of the NASA Infrared Telescope Facility (IRTF) spectral observations of human-made space objects taken from 2006 to 2008. The data collected using the SpeX infrared spectrograph cover the wavelength range 0.7-2.5 μm. Overall, data were collected on 20 different orbiting objects at or near the geosynchronous (GEO) regime. Four of the objects are controlled spacecraft, seven are non-controlled spacecraft, five are rocket bodies, and four are cataloged as debris pieces. The remotely collected data are compared to the laboratory-collected reflectance data on typical spacecraft materials; thereby general materials are identified but not specific types. These results highlight the usefulness of observations in the infrared by focusing on features from hydrocarbons and silicon. The spacecraft, both the controlled and non-controlled, show distinct features due to the presence of solar panels whereas the rocket bodies do not. Signature variations between rocket bodies, due to the presence of various metals and paints on their surfaces, show a clear distinction from those objects with solar panels, demonstrating that one can distinguish most spacecraft from rocket bodies through infrared spectrum analysis. Finally, the debris pieces tend to show featureless, dark spectra. These results show that the laboratory data in its current state give excellent indications as to the nature of the surface materials on the objects. Further telescopic data collection and model updates to include noise, surface roughness, and material degradation are necessary to make better assessments of orbital object material types. However, based on the current state of the model, infrared spectroscopic data are adequate to classify objects in GEO as spacecraft, rocket bodies, or debris.

1. INTRODUCTION

One of the roles of the NASA Orbital Debris Program Office at Johnson Space Center (JSC) is to characterize the debris environment through the assessment of the physical properties (type, mass, density, and size) of objects in orbit. Knowledge of the geosynchronous orbit (GEO) debris environment, in particular, can be used to determine the hazard probability at specific GEO altitudes and aid predictions of the future environment. Currently, an optical size is calculated using an assumed albedo for an object and its intensity measurement. However, identification of specific material type or types could improve albedo accuracy and yield a more accurate size estimate for the debris piece. Using spectroscopy, it is possible to determine the surface materials of space objects.

2. DATA COLLECTION AND REDUCTION

2.1 Telescope Observations

Observations of orbital objects were taken with the 3.0-meter telescope at the NASA Infrared Telescope Facility (IRTF) using the SpeX [1] instrument on 26-29 October 2006, 26-28 June 2007, 25-26 November 2007, and 5 May 2008. SpeX was used in low resolution (prism) mode and the slit width was 0.8″. The data from the nights reported herein were spectrophotometric. In this configuration, the instrument provides a spectral resolution ($\lambda/\Delta\lambda$) of ~93 across the entire 0.7- to 2.5-μm wavelength range. Signal-to-noise values of the data obtained by SpeX are contingent on the brightness of the object at the time of observation, the total integration time, and the atmospheric conditions at the summit. The signal-to-noise values for most objects observed with this instrument are attainable in excess of 80 to 100, given good viewing conditions. See Abercromby, Abell, and Barker [2] for more details on the instrument and telescope.

Over the course of these observations, spectral data were acquired on subset of cataloged GEO targets from the U.S. Space Surveillance Network (SSN) database. These objects included rocket bodies, functional spacecraft, non-functional (NF) spacecraft, and orbital debris. The NF targets are no longer controlled in the east-west direction and the inclination is allowed to increase (see Table 1~~Table 1~~ for a summary of all observations). The table heading listed as NF refers to targets that are nonfunctional; the orbit is no longer controlled in the East-West direction, and the inclination is allowed to increase. Once a GEO satellite is no longer controlled, the inclination will vary by 15º over a 50-year cycle due to orbital perturbations. In four cases, the same object was observed on multiple campaigns. During the course of a night's observation campaign calibration data were acquired, including flats, arc lamps (wavelength calibration), atmospheric standards (telluric feature removal), and solar analogs (for relative reflectance ratios). Typically, exposure time sets for the SSN objects were 45 seconds placed in pairs, where the object was shifted 1" up and down the slit (necessary for sky emission removal and bias/dark removal). Only two solar analogs were used throughout the 2-year campaign, SAO 93936 and SAO 120107.

Table 1. IRTF SpeX Observation Summary

SSN Number	Common Names	International Designator	26-29 Oct. 2006	26-28 June 2007	25-26 Nov. 2007	5 May 2008	NF?
08476	SATCOM 1	1975-117A	X				Yes
08832	TITAN 3C TRANSTAGE DEB	1976-023J				X	Yes
11669	OPS 6393 (FLTSATCOM 3)	1980-004A	X				Yes
11964	GOES 4	1980-074A	X				Yes
12855	SBS 2	1981-096A		X			Yes
13984	SATCOM 1R	1983-030A				X	Yes
14234	ARABSAT 1DR (TELSTAR 3A)	1983-077A	X				No
14421	INTELSAT 507	1983-105A	X				No
15385	SPACENET 2	1984-114A	X			X	No
15826	TELSTAR 303	1985-048D	X				No
19550	IUS R/B (2)	1988-091D			X		Yes
20570	NEWSAT-1 (PALAPA B2R)	1990-034A			X		Yes
21641	IUS R/B (2)	1991-054D		X	X	X	Yes
21648	COSMOS 2054 DEB	1989-101G		X			Yes
22316	IUS R/B (2)	1993-003D		X			Yes
23615	IUS R/B (2)	1995-035D			X		Yes
25000	TITAN 3C TRANSTAGE DEB	1968-081G				X	Yes
25126	HGS-1 (ASIASAT 3)	1997-086A	X				Yes
25645	SL-12 R/B (2)	1999-010D		X		X	Yes
29014	EKRAN 2 DEB	1977-092K	X				Yes

The data were reduced using Spextool [3]. The typical settings outlined in [4] were used to minimize issues with the data's complexities. One first starts with the IDL command *xspextool* to perform reduction, calibration, and extraction. We used the Point Source tab exclusively for these data with additional inputs to the paths to the image and calibration data on the computer. This tab combines all the necessary calibration steps (flat field correction, wavelength calibration, defining apertures for extraction, tracing emission of the object across the array, and finally, extracting 1-D spectra). Combination of 1-D spectra for an individual object was performed with Spextool's *xcombspec* procedure. This procedure scales the individual spectra (greyscaling in optical spectra jargon). We combined spectra using a robust weighted mean with 8σ threshold and a limited wavelength range of 1.17-1.32 μm. The wavelength range was chosen because the signal-to-noise over this range is the highest and because this wavelength range has minimal telluric line contamination. Atmospheric standard star spectra were taken before and after each associated debris object, and often solar analogs were observed more than once per night. For the standard stars, spectra was combined depending on when the star was observed: before the object observation, after the object observation, and a combination of both sets. Finally, the spectra on debris objects and solar analogs had the telluric absorption features removed using Spextool's *xtellcor_basic* procedure. To get the most out of the elimination of these telluric features, only the 1.3-1.4 μm feature was used in the procedure so that the standard deviation of the residual wavelength shifts given in the output of the procedure's model was only due to residuals from an absorption feature. Spextool does not

allow several disjointed wavelength regions to be chosen. The standard deviation of the residual wavelength shifts was compared between the three types of atmospheric standard star summations. The one that gave the smallest standard deviation was used with that orbital debris object and solar analog.

Once the steps above were completed, the relative reflectance ratio spectra of the objects were produced. These images were produced by ratioing the object and solar analog star. To insure sky conditions are completely removed from the image, both the object spectra and solar analog spectra were ratioed by the standard star spectra closest in time and position to the object observations. This procedure gives us a final ratio of the SSN to solar analog where the atmospheric lines have been eliminated completely. An example of this ratio can be found in Fig. 1~~Fig. 1~~.

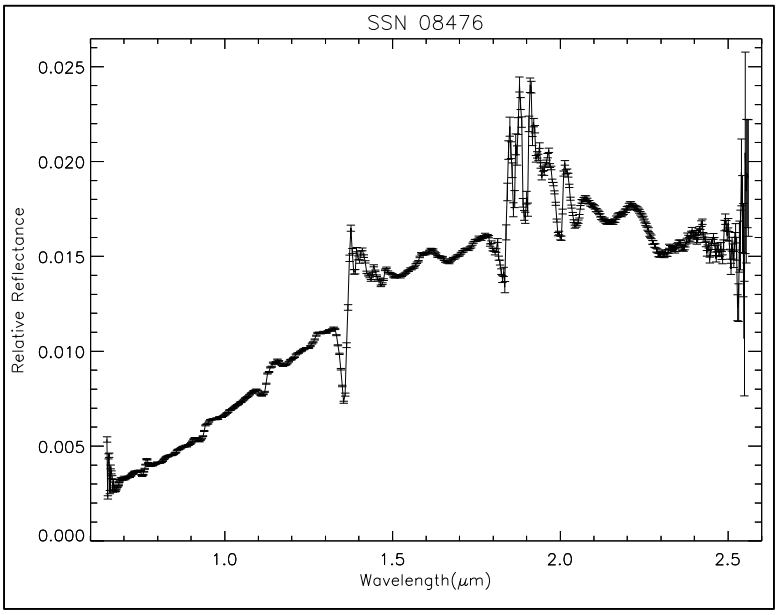

Fig. 1. SSN 8476 spectral data acquired 28 October 2006. The y-axis is relative reflectance, and the x-axis is wavelength in microns. Large spikes (e.g., between 1.8 and 2.0 μm) are indicative of residuals left over from removing telluric features. Ratioing to a solar analog has not occurred so useful information about materials cannot be made from this graph.

2.2 Laboratory Data

When collecting data in a laboratory, a white reference is measured and compared to the material spectrum such that the resulting spectrum is called an absolute reflectance measurement that is on the scale of zero to one. However, there is not such an absolute reflectance standard at the same distance and orientation of each of the satellites. Therefore, the data are considered as relative reflectances. In these cases, the shape of the spectrum and the location and strength of the absorption features are used to determine material and not the percent reflectivity. To be able to compare measurements from two different objects, it may be necessary to scale to the object's reflectance so that both reflectances fit on one plot. When this practice was done, it will be noted.

An Analytical Spectral Device field spectrometer that has a wavelength range from 0.3 to 2.5 microns (μm) with a resolution of 10 nanometers at a wavelength of 2 μm and 717 channels was used to obtain the laboratory measurements. From these laboratory measurements, a database of more than 300 common spacecraft materials reflectance spectra was assembled and is used for comparison with the IRTF remote observations to determine material type [5]. All of the laboratory data referred to on the figures in this paper are from the NASA Spectral Database [5].

For these comparisons, the objects were known, catalogued pieces and thus the authors had *a prior* knowledge as to what materials would be best to include when comparing the remote data to lab data. However, some non-traditional materials were included as well such that the list is shown in

Table 2~~Table 2~~. All of the solar cells are different in type; not all the types are known and those that are not known are typed generically. The exposed white paint is white paint that was flown on the Long Duration Exposure Facility; the paint turned a gold color with exposure to the environment [5].

Table 2. List of Materials for Comparison

Material		
Solar Cell Montana (MT)	Inconel (nickel-chromium superalloy)	Carbon Epoxy
Solar Cell Polysat	Anodized Aluminum	White Paint
Solar Cell at 0 deg phase	Aluminum Beta Cloth	Exposed White Paint
Solar Cell TRMM	Aluminized Kapton	Multi-Layer Insulation— Kapton

3. SPECTRAL UNMIXING

Spectral unmixing is the process of inverting material proportions from a combined spectrum that has distinct components that are linearly mixed. Rapp [6] developed a Constrained Linear Least Squares (CLLS) model with the application of unmixing reflectance spectral data of orbiting objects. Spectra are added linearly according to the proportion represented on the surface of the object. Considering orientation of incident light and the object, the full equation defining the combined spectrum in terms of orientation [6, 7] is:

$$S_{combined} = \sum_{i=1}^{n} p_i B_i S_i + N$$

where S is a spectrum, i is an index representing the i^{th} material, p is the material proportion of the full spectrum, N is noise, and B_i is the orientation coefficient for the i^{th} material. This equation is still an approximation, however, as the orientation can change the spectrum. It should be noted that $S_{combined}$ and S_i can be represented as very long vectors, with reflectance values at each of the measured wavelengths. This allows an expansion into a vector math representation:

$$\vec{S}_{combined} = p_1 B_1 \overrightarrow{S_1} + p_2 B_2 \overrightarrow{S_2} + \cdots + p_n B_n \overrightarrow{S_n} + \vec{N}$$

where p_i and B_i are both scalars, making it quite easy to restate this as a matrix multiplication problem with a known solution:

$$S_c = SA$$

Unfortunately, the matrix S is not square so it cannot be truly inverted to solve directly for A so a pseudo-inverse can be used. When applied to this problem this inverse is known as a least-squares optimization:

$$S^T S_c = S^T S A$$

Multiplying both sides by S^T creates a square matrix that is guaranteed to be invertible:

$$(S^T S)^{-1} S^T S_c = A$$

This function minimizes the equation and provides a beginning point for the solution to the unmixing problem. Testing this solution, for some combined spectra the unmixer returned negative proportion values, which is physically impossible. This is because the model is trying to match shape and subtracting materials can be the same as adding in terms of the final result. To rectify this issue a constrained least squares function was used, MATLAB's built in *lsqnonneg* function. The function uses a modified Lagrange multiplier method to solve the constrained problem. By reframing this as a vector problem, and recognizing it as a minimization problem, it becomes clear that the Lagrange solution is solving the constrained minimization problem:

$$f = (S_c - SA) \;\; A \geq 0$$

This is solved for the specific $A \geq 0$ case by the *lsqnonneg* function. To maintain the constraint using a Lagrange multiplier method, the function first calculates the least squares solution, including negative solutions. It then uses those solutions to create a vector of logicals defining which solutions are negative, and need to be corrected. This vector becomes the Lagrange multiplier, and the optimization is performed. This process is repeated until an optimum solution is found.

To estimate the error in the results when unknown spectra are unmixed, the difference between the original and unmixed spectra is calculated (called the residual). Since a vector approximation method is used to calculate the best

unmixing solution, the norm is calculated, and used for error. This area is then used to calculate the error based on the difference in area.

$$E = \frac{Norm_{diff}}{Norm_{orig}} = \frac{\sqrt{S_{diff}^T S_{diff}}}{\sqrt{S_c^T S_c}}$$

This error estimation gives a percentage error, and gives an estimation of the cut-off point of significant figures in the output. This model takes all the materials supplied and creates the best, combined spectrum based on the above method.

4. RESULTS

The remotely collected data are compared to the laboratory-collected reflectance data on typical spacecraft materials; thereby general materials are identified but not specific types. Each spectral image shown contains the remote data on the object and the spectral unmixing program (CLLS) spectrum. In addition, a simple subtraction between the two spectra is also shown on the plots. This difference is calculated at each wavelength. The overall error (shown in the calculations in the previous section) is listed in the figure captions.

Spectral data on object SSN20570 (NEWSAT-1 [PALAPA B2R]) is shown in Fig. 2~~Fig. 2~~. Both model data and the remote data are scaled such that their reflectances are compared. The matching materials used in CLLS were multi-layered insulation (MLI), solar cell, anodized aluminum, Inconel, white paint, and exposed white paint. The model fits the original data to within 1% and this error is the lowest of all the data presented. Solar cells have a band gap feature near 1100 nm, as seen in the original and unmixed data in Fig. 2~~Fig. 2~~. These results are consistent with the satellite design, which is a cylindrical bus-type covered in solar cells, similar to Fig. 3~~Fig. 3~~. In addition to the solar cell feature, common features due to carbon-hydrogen (C-H) are seen near 1700 nm and 2400 nm in both the CLLS model and remote data. The laboratory data tend to have some of the water features present (seen in Fig. 2~~Fig. 2~~ near 1400 and 1900 nm); however, the remote data have them completely removed due to the amount of water in the atmosphere. This makes it difficult to assess when the water features are due to the atmosphere and when they are from the spacecraft. Therefore, the features are removed completely such that an erroneous statement of water being present is not made. Thus, those regimes will never agree with the CLLS model in any of the figures shown. In future work, the intent is to remove the features from the laboratory data and redo the comparison.

The spectral data were analyzed using the Image Reduction and Analysis Facility software package to identify the spectral features found in each remote observation. .

Table 3~~Table 3~~ lists the wavelengths of the identified feature(s) and the full widths at half maximum (FWHM) in nanometers compared with the FWHM found in the CLLS model. These prominent features identified in the table are consistent with C-H bonds commonly found in organics. These numbers show that the model has not obtained the exact correct materials or concentration of material correct for comparison. These are a few of the reasons that all percent errors between the data and the model are greater than 1%.

Three of the four functional spacecraft observed showed similar results to Fig. 2~~Fig. 2~~. Large band gaps were seen at 1100 nm due to solar panels and organic features seen at 1700, 2100, and 2300-2400 nm. It is believed that the orientation of and/or solar angle relative to the fourth spacecraft is the reason for the dissimilar results.

Object SSN08476 (SATCOM 1) did not compare well to the CLLS model. As shown in Fig. 4~~Fig. 4~~, the absorption feature seen in solar cell materials near 1100 nm is not present in the original data. The percent error ranged from 10-13% depending on the type of solar panel used in the model. Although the satellite has large solar panels present, the aspect angle during the observation may have been such that the recorded spectrum was of another part of the spacecraft (see Fig. 5~~Fig. 5~~). This satellite is nonfunctional and could potentially be tumbling or rotating. The CLLS model did find the C-H features near 1700 and 2400 nm again, indicating that there are organics found on the spacecraft, but that the materials shown in the remote spectra are not found in those used with the CLLS model. To highlight those differences, the FWHM values are shown in
Table 4~~Table 4~~. Not only are the values wide ranging, the location of those wavelengths centers are also different. Again, more material information is necessary.

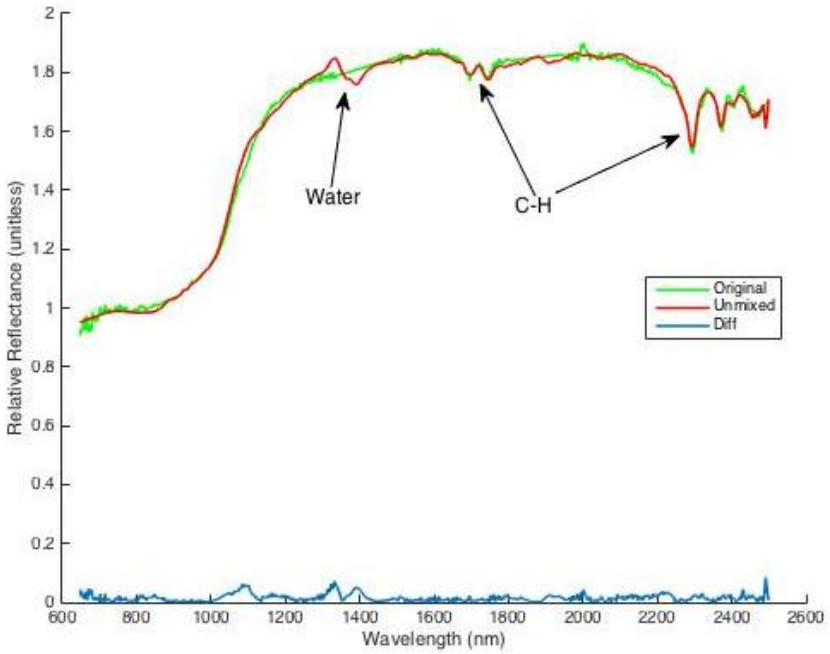

Fig. 2. Spectral Data from SSN20570. Green line is the original data, red line is the model fit to the data, and blue is the difference between the green and red lines. The percent error is less than 1%. The largest variations occur around the water features and the organic features.

Fig. 3. Palapa-B image. This is an artist rendition of a HS 376 communication satellite.
Ref: http://space.skyrocket.de/doc_sdat/palapa-b.htm.

Table 3: Comparison of FWHM for the model and the original data

SSN	Central Wavelength (nm)	FWHM (nm)	Central Wavelength model (nm)	FWHM model (nm)
ssn20570 (Nov2007)	1700	21	1699	23
ssn20570	1740	20	1745	30
ssn20570	2290	32	2291	47
ssn20570	2370	18	2369	23

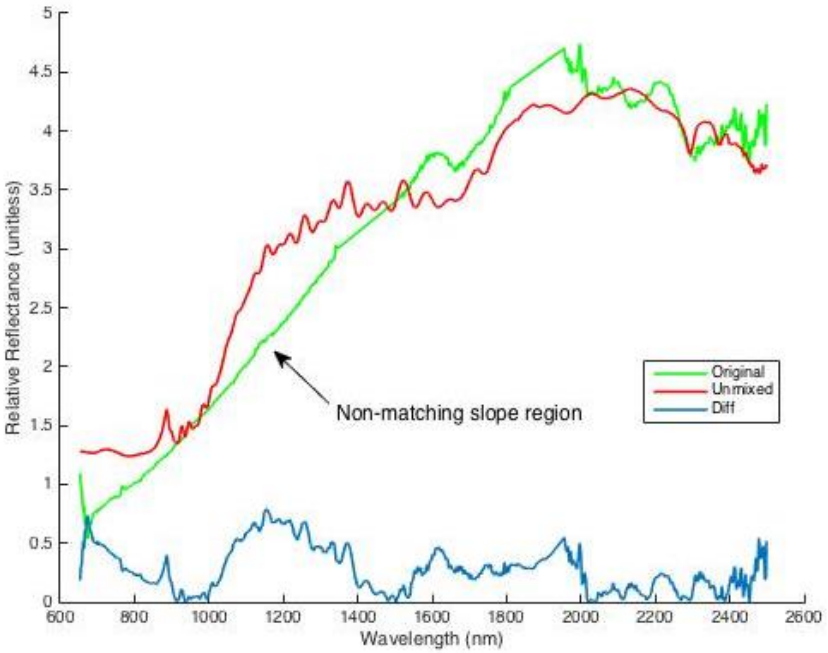

Fig. 4. Spectral Data from SSN08476. Green line is the original data, red line is the model fit to the data, and blue is the difference between the green and red lines. The percent error is 10-13% depending on the solar panel material chosen. The major difference is the non-matching slope through the near IR—especially the silicon feature at 1100 nm.

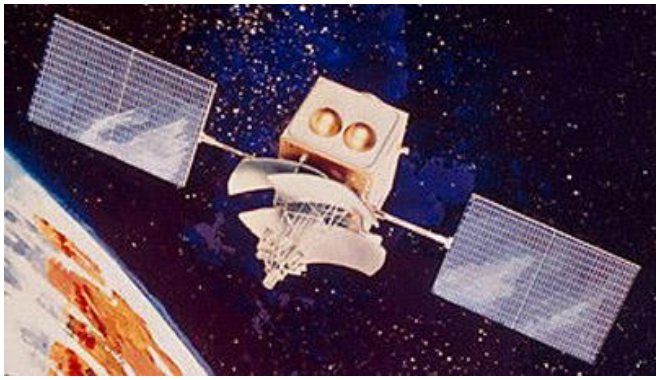

Fig. 5. Satcom 1 image. Ref: http://space.skyrocket.de/doc_sdat/satcom-1.htm

Table 4: Comparison of Absorption Features for SSN 8476

SSN	Central Wavelength (nm)	FWHM (nm)	Central Wavelength model (nm)	FWHM model (nm)
ssn08476	1690	90	1738	23
ssn08476	2150	58	2176	35
ssn08476	2310	86	2292	47
ssn08476	2450	31	2370	23

To highlight an example that does not have solar panels, the results from SSN22316 are shown in Fig. 6~~Fig. 6~~. The SSN22316 is an Inertial Upper Stage (IUS) rocket body and is shown in Fig. 7~~Fig. 7~~. The slope seen through the visible (600-800 nm) regime does not match that seen in intact spacecraft (see Fig. 6~~Fig. 6~~, both images). However, the CLLS model was able to detect the C-H features and the general slope to within 2.5%. With *a priori* knowledge that no solar cells existed on this sample, the CLLS model was run again without solar panels, and the results are

shown in Fig. 6~~Fig. 6~~, right image. The materials that matched the remote data the best were anodized aluminum, white paint, and white exposed paint (left image of Fig. 7). Fig. 7~~Fig. 7~~ shows the entire rocket body and not just the final stage that resides in GEO. That stage may display significant properties of Kevlar (motor case) and carbon/carbon (nozzle). Neither material is represented in the current material database.

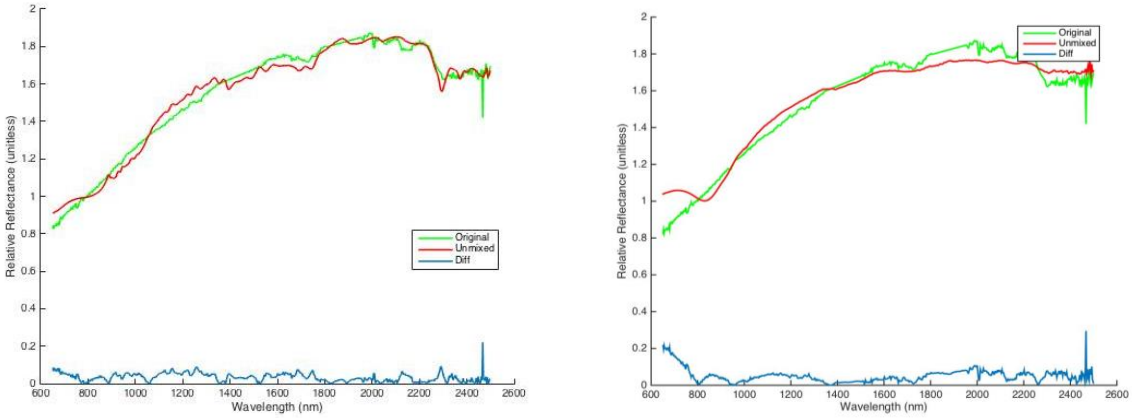

Fig. 6. CLLS and original data for SSN22316, the IUS rocket body, left image has solar panels in the unmixed materials spectrum and the right image does not have solar panels in the unmixed spectra. Green line is the original data, red line is the model fit to the data, and blue is the difference between the green and red lines. Please note that the percentage difference is smaller in the left image.

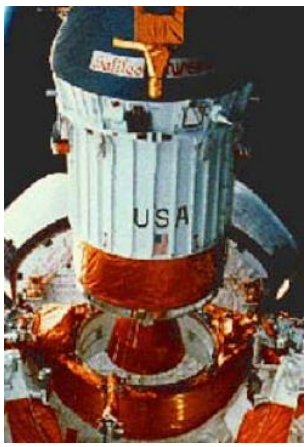

Fig. 7. IUS rocket body (photo credit: NASA.gov)

The CLLS had the hardest time matching materials with the orbital debris pieces. Fig. 8~~Fig. 8~~ and Fig. 9~~Fig. 9~~ show data from Titan Transtage debris (SSN25000) and the Ekran 2 debris piece (SSN29014), respectively. The CLLS model did not have materials in the database to match the debris pieces. Fig. 8~~Fig. 8~~ shows a relatively featureless although increasing slope spectrum with a match to aluminum and solar panel at 4% error. Fig. 9~~Fig. 9~~ shows more absorption features at 1700 and 2300 nm but nothing that matches well in the database and shows a 7% error. In both samples, aluminum was the dominant match. As in the previous example, the CLLS model was run again without solar panels in the material selection and the materials used in the best fit were aluminum and exposed white paint for both SSN 25000 and SSN 29014, and again, aluminum was the dominant material. However, the error increased to 8 and 16%, respectively. The authors think that solar panels are not in these objects, but some material with similar spectral response that is not in the database and model is present in the relative reflectance spectra.

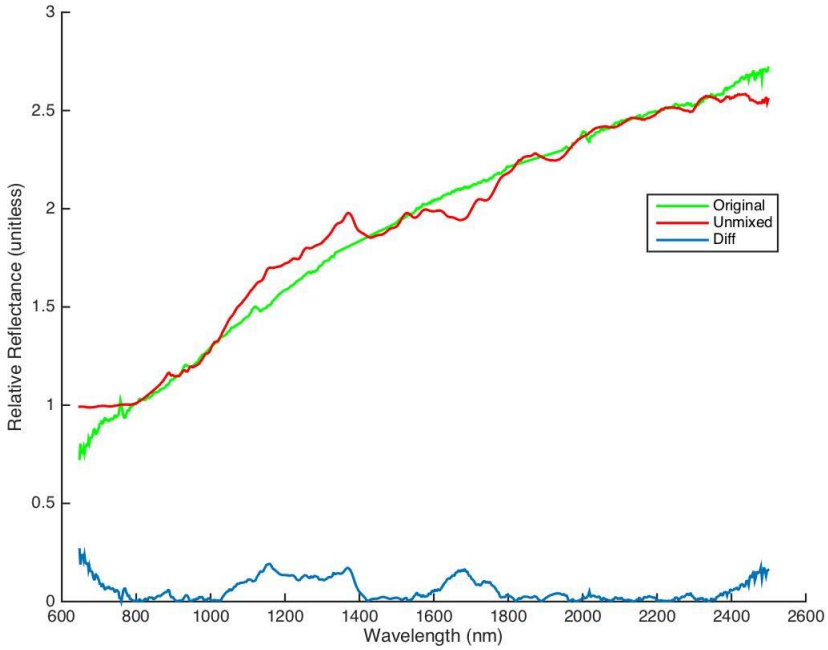

Fig. 8. Titan debris (SSN25000) remote data compared to CLLS model data with a 5% error. Green line is the original data, red line is the model fit to the data, and blue is the difference between the green and red lines.

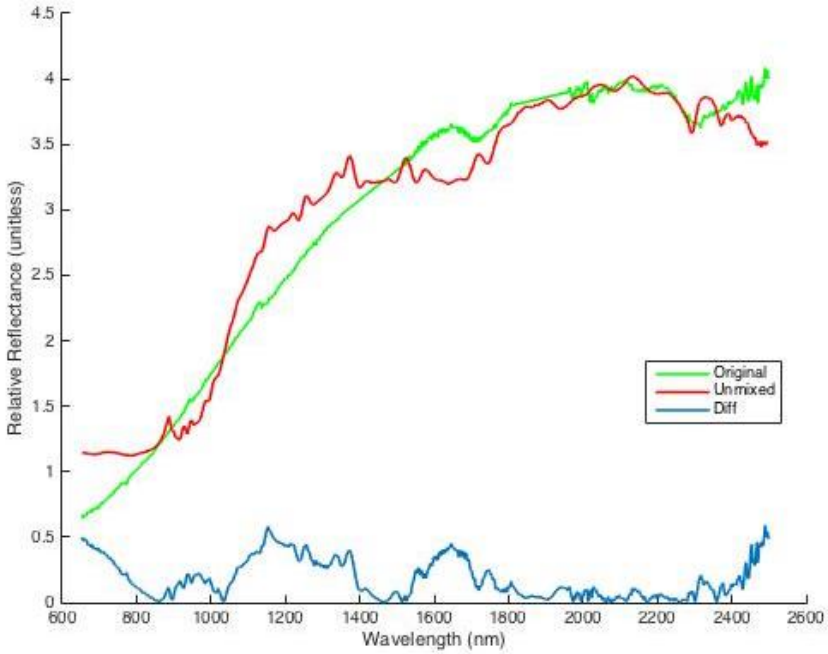

Fig. 9. Ekran Debris remote data compared with the CLLS model with a 7% error. Green line is the original data, red line is the model fit to the data, and blue is the difference between the green and red lines.

Overall, the CLLS model showed promising results. Since all of the images could not be shown in the paper, a review of the materials identified and the percent error is shown in Table 5~~Table 5~~. The dominant material found was solar cells. The debris objects had higher error values showing that the model does not contain the materials shown in the remote sample. The differences between the results between an intact spacecraft, rocket body, and debris piece are evident by the material selected.

Table 5: Details of the material matches for the objects observed

SSN	Common Name	Materials Found	%error
08476	SATCOM 1	Solar Cell, Aluminum	9%
08832	TITAN 3C TRANSTAGE DEB	Solar Cell, Aluminum	7%
11669	OPS 6393 (FLTSATCOM 3)	Solar Cell, Aluminum	6%
11964	GOES 4	Solar Cell	5%
12855	SBS 2	Solar Cell, MLI, Kapton, White paint, Exp white paint, Inconel	1%
13984	SATCOM 1R	Solar Cell, MLI, Kapton, White paint, Inconel	2%
14234	ARABSAT 1DR (TELSTAR 3A)	Solar Cell, MLI, Alumized Kapton, White paint, Inconel	2%
14421	INTELSAT 507	Solar Cell, Aluminum	5%
15385	SPACENET 2	Solar Cell, MLI, Kapton, White paint, Exp white paint, Inconel	2%
15826	TELSTAR 303	Solar Cell, MLI, Kapton, White paint, Exp white paint, Inconel	1.5%
19550	IUS R/B (2)	Exp White paint	7%
20570	NEWSAT-1 (PALAPA B2R)	Solar Cell, MLI, Aluminum, Kapton, White paint, Exp white paint, Aluminized Beta Cloth	1%
21641	IUS R/B (2)	Exp White paint	8%
21648	COSMOS 2054 DEB	Solar Cell, MLI, Kapton, White paint, Exp white paint, Inconel	2%
22316	IUS R/B (2)	White paint, exp white paint	3%
23615	IUS R/B (2)	Aluminum, exp white paint	5%
25000	TITAN 3C TRANSTAGE DEB	Anodized Aluminum, Solar cell	4%
25126	HGS-1 (ASIASAT 3)	Solar Cell, MLI, Kapton, White paint, Exp white paint, Inconel	4%
25645	SL-12 R/B (2)	Aluminum, Aluminized Kapton, Exposed White paint	3%
29014	EKRAN 2 DEB	Aluminum, Solar Cell	4%

5. CONCLUSIONS

Spectral data taken at IRTF during 2006 to 2008 were shown and compared to a constrained linear least squares model using common spacecraft materials. The data collected using the SpeX infrared spectrograph cover the wavelength range 0.7-2.5 μm. Overall, data were collected on 20 different orbiting objects at or near the GEO regime. Four of the objects were controlled spacecraft, seven were non-controlled spacecraft, five were rocket bodies, and the final four were cataloged as debris pieces. The dominant material found was solar cells. The debris objects had higher error values showing that the model does not contain the materials shown in the remote samples. The differences between the results of an intact spacecraft, rocket body, and debris piece are evident. The spacecraft, both the controlled and non-controlled, show distinct features due to the presence of solar panels, whereas the rocket bodies do not, as expected. Signature variations between rocket bodies, due to the presence of various metals and paints on their surfaces, show a clear distinction from those objects with solar panels, demonstrating that one can distinguish most spacecraft from rocket bodies through infrared spectrum analysis. Future work on this topic includes adding more noise to the model such as surface roughness, examining the phase angles in conjunction with the spectra, and adding more laboratory materials to the model in hopes of more clearly defining the material types of these objects. Due to the wide variation of materials used on spacecraft, coatings applied to those materials, and space environmental effects while on orbit, having a perfect match between laboratory data and remote data would be impossible. However, the inclusion of more materials into the model and including space environmental and material degradation effects as well will increase the likelihood of determining the material types of these orbiting objects.

7. ACKNOWLEDGEMENTS

The authors would like to thank Bill Golisch and Dave Griep for operating the NASA IRTF and facilitating the collection of the spectral data. Kira Abercromby and Paul Abell are visiting astronomers at the Infrared Telescope Facility, which is operated by the University of Hawai'i under Cooperative Agreement no. NCC 5-538 with the National Aeronautics and Space Administration, Science Mission Directorate, Planetary Astronomy Program.

8. REFERENCES

1. Rayner, J. T., *et al.*, SpeX: A medium-resolution 0.8-5.5 micron spectrograph and imager for the NASA Infrared Telescope Facility. *Publications of the Astronomical Society of the Pacific*, 115, 362-382.
2. Abercromby, K.J., *et al.*, Reflectance Spectra Comparison of Orbital Debris, Intact Spacecraft, and Intact Rocket Bodies in the GEO Regime, *European Conference on Space Debris*, April 2009.
3. Cushing, M., *et al.*, Spextool: A Spectral Extraction Package for SpeX, a 0.8-5.5 micron Cross-Dispersed Spectrograph, Publications of the Astronomical Society of the Pacific, Vol. 116, 362, 2004.
4. Vacca, W., *et al.*, A Method of Correcting Near-Infrared Spectra for Telluric Absorption, Publications of the Astronomical Society of the Pacific, Vol. 115, 389, 2003.
5. NASA JSC Spacecraft Materials Spectral Database, NASA JSC, 2004.
6. Rapp, J., Identification of Orbital Objects by Spectral Analysis and Observation of Space Environment Effects, Master's Thesis, California Polytechnic State, San Luis Obispo, September 2012.
7. Keshava, N. and Mustard, J. F., Spectral Unmixing. *IEEE Signal Processing Magazine* , 44-57, January 2002.